Chapter

Long-Term Behavior of Coarse-Grained Rockfill Material and Their Constitutive Modeling

Erich Bauer

Abstract

For the long-term behavior and safety assessment of rockfill dams, not only the shape of the dam body, the loading history, the geological condition of the dam foundation and abutments, the assessment of possible seismic hazards and seepage events caused by defects of the sealing are important, but also the time dependent mechanical behavior of the dam materials used can be of significant influence. In this paper a novel hypoplastic constitutive model for moisture sensitive, coarse-grained rockfill materials is presented. In the constitutive equations, the so-called solid hardness is a key parameter to reflect the influence of the state of weathering on the mechanical response. With respect to the evolution equation for the solid hardness, creep and stress relaxation can be modeled for dry and wet states of the material in a unified manner. The performance of the model is demonstrated by comparing the numerical simulation with experimental data.

Keywords: rockfill material, wetting behavior, creep, stress relaxation, hypoplasticity

1. Introduction

Rockfill dams have become very popular among dam engineers due to of their simple construction sequence, short construction period and low costs compared to concrete dams. An economic aspect also lies in the fact that rockfill materials of different types are usually available on site can be used in appropriate zones of the dam. The frequent use of weathered and moisture-sensitive rockfill materials requires the precise recognition of the mechanical behavior of these materials under the expected load and environmental conditions. The prediction of the post-construction settlements of rockfill dams is a challenging task because of uncertainties of environmental events, which can occur during the entire lifetime of the dam [1, 2]. Changes of the moisture content of weathered rockfill material can lead to sudden settlements that could have relatively large values, without any changes in the applied load [3–8]. For the long-term behavior of rockfill dams, not only the shape of the dam body, the loading history, the geological condition of the dam foundation and abutments, the assessment of possible seismic hazards and seepage events caused by defects of the sealing are important, but also the time dependent behavior of the dam materials used can be of significant influence [9–11]. Thus, the proper modeling of the time dependent behavior of rockfill material under different

loading and environmental condition plays an important role for the design, construction, operation and safety assessment of rockfill dams. For instance, post construction settlements may affect the amount of the bending and the crack propagation in concrete slaps of concrete face rockfill dams [12–16].

In engineering disciplines time dependent deformations under constant stress are termed creep, however, this term does not reflect the individual mechanisms that different types of materials can exhibit. Rheological properties of weathered rockfill materials are strongly influenced by the state of weathering and the mechanical and environmental boundary conditions to which the material is subjected. Thus, the concept for the experimental investigations requires an appropriate adaptation to the conditions relevant at the construction site. In this context also scale effects resulting from the differences between the grain size distribution and pre-compaction in laboratory tests and in the filed must be taken into account [17–19].

Long-term deformations are usually an accumulation of deformations related to various events and the proper interpretation of the relevant physical and hydro-chemical mechanisms is important for the evaluation of the data obtained from laboratory experiments and field measurements as well as for the numerical modeling. A general distinction can be made between time independent deformations, which are the instantaneous part of the deformation due to applied load changes, and time dependent deformations, which can also take place under constant load. The former, for instance, can be initiated by rapid changes of the water level in the reservoir, the change of the effective stresses caused by a change of suction of fine grained materials, hydraulic fracturing and piping as a result of the seepage-driven internal erosion of solid particles. Time dependent deformations are influenced by the mineralogical composition of the solid material, the frequency and the orientation of micro-cracks, the grain size distribution, the pre-compaction, the moisture content, the stress state and the evolution of weathering [20–24]. Progressive weathering caused by mechanical and hydro-chemical weathering has a significant influence on the time dependent process of the degradation of the solid hardness and as a consequence on the resistance of the material against compaction and shearing. In dam engineering it is common to differentiate between long-term creep and so-called collapse settlements. While the former is related to the rheological properties of the rockfill material and controlled by gravity load and the effect of water impounding, the latter can usually be observed immediately after a change of the moisture content in the stressed rockfill material. Collapse settlements are also called instantaneous wetting deformation and characterized by a spontaneous increase of the deformation velocity.

Changes of the moisture content can be caused by different events like climate changes, leakage as an effect of defects of the dam sealing and the dam foundation, as well as by rainwater infiltration into the dam body. According to Terzaghi [25] collapse phenomenon are also time dependent and related to the decrease in the grain crushing strength, especially at the contact points. Plastification of grain contacts and grain crushing bring about local instabilities in the grain skeleton. Rheological properties of weathered rockfill materials are more pronounced in the wet state of the material than in the dry state [4, 9, 11, 26]. Depending on the state of weathering of the rockfill material a change of the moisture content can initiate an acceleration of the crack propagation of stressed rockfill grains, which leads to a reduction of the solid hardness and consequently to a sudden increase of the settlement velocity. **Figure 1a** shows an example for an increase of the settlement velocity after flooding under a constant vertical stress of −0.8 MPa in an oedometer device [3]. The course of the deformations is qualitatively similar for greywacke and sandstone and can be divided into three parts. After applying the vertical stress on

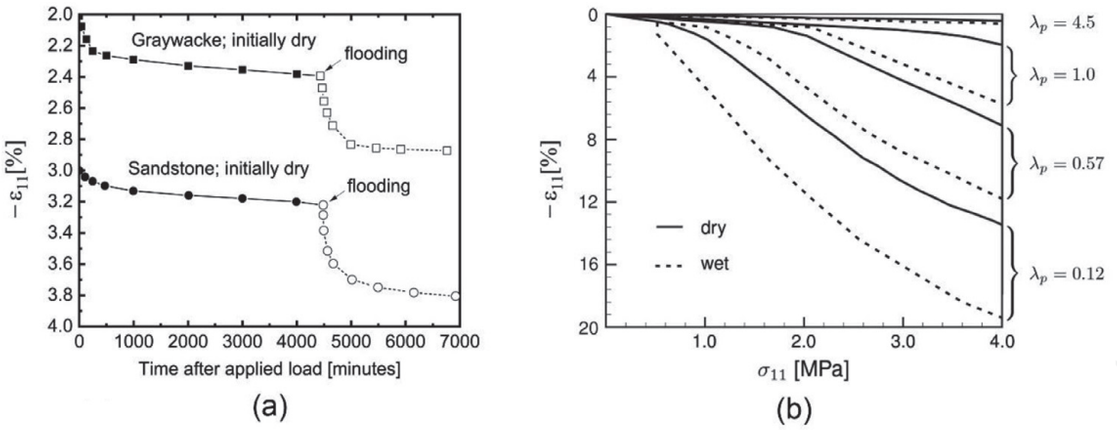

Figure 1.
(a) Time dependent behavior of two different rockfill materials under a constant vertical stress of −0.8 MPa in an oedometer device carried out by Sowers et al. [3]; (b) oedometric compression behavior of broken granite under dry and water saturated conditions and for different pre-compactions [27, 28] (herein λ_p denotes a measure of the relative pre-compaction energy).

the initially dry material, an instantaneous settlement can be detected, which is larger for sandstone. Under constant stress, creep can be observed in the dry state and also following a sudden flooding of the specimen. Flooding leads to a sudden jump of the settlement rate but there is no clear sharp jump in the settlement which indicates that so-called collapse settlements can also assumed to be time dependent. While for the dry material the creep velocity decreases slowly, the high settlement rate immediately after flooding fades out very fast. It is experimentally evident that the compressibility of weathered rockfill material strongly depends on the pre-compaction and moisture content of the material, i.e. the compressibility is higher for a less compacted material and higher for the wet than for the dry material. This is also clearly visible for example from the results of oedoemeter compression tests with weathered broken granite in **Figure 1b** [27, 28]. Great efforts have been made to investigate and to model the complex mechanisms of wetting deformations at the micro- and macro-level, e.g. [29–46].

The focus of this paper is on the time dependent process of degradation of the stiffness of weathered, coarse grained and moisture sensitive rockfill materials and its constitutive modeling under dry and wet states. A particular version of a hypoplastic model developed within the past decade is presented and its performance is verified by comparison of numerical simulations with experimental data. It is an aim of the present paper to propose simple calibration procedures for the material parameters based on standard laboratory tests. As a measure of the state of weathering the so-called "solid hardness of the grain assembly" is a key parameter in the material model proposed [47–52]. Particular attention is paid on a refined modeling of the influence of the coupled behavior between the state of weathering, the stress state and the packing density of the rockfill material on the calibration of those material parameters relevant for collapse settlements, long-time creep and stress relaxation. In this context the modeling of the change of the rheological material parameters during the lifetime of the dam, the concept of the solid hardness is put forward to simulate a repeated acceleration of the degradation of the solid hardness. Such events are relevant for repeated changes in the moisture content of the rockfill material caused by local defects of the sealing and heavy rain water infiltration into the rockfill material of the dam body. While the focus of the present paper is on the theory of constitutive modeling and its calibration, the application of the proposed material model to different types of rockfill dams can be found for instance in [53–56].

The present paper is organized as follows:

In Section 2 resent developments of modeling the compression behavior of weathered, creep and moisture sensitive rockfill materials under dry and wet condition are summarized. To this end the so-called "solid hardness" is defined in the sense of a continuum description and is a state parameter in Bauer's compression law [47, 57, 58]. As an example of how the concept of the solid hardness can be incorporated into a general three dimensional material model the adaptation of the compression law to the bulk modulus of a nonlinear elastic material model is outlined. In incrementally non-linear material models, for instance, the concept of the solid hardness was embedded into non-polar constitutive models, e.g. [58–60] and into micro-polar models, e.g. [61–68]. In the present paper the proposed enhanced constitutive model for the solid hardness is a time dependent quantity and a measure of the state of weathering of the rockfill material [47]. With respect to the evolution equation of the time dependent process of degradation of the solid hardness creep and stress relaxation are modeled in a unified manner. Particular attention is paid to the adaptation of the velocity parameter in the evolution equation of the solid hardness to experimental creep and stress relaxation curves.

Section 3 gives a brief introduction to the hypoplastic constitutive model by Gudehus [69] and Bauer [58] which was originally developed for a constant solid hardness and a time independent material behavior. The incrementally nonlinear constitutive equation describes the stress rate as a function of the current void ratio, the Cauchy stress and the strain rate. In contrast to the concept of elasto-plasticity, the framework of hypoplasticity does not need to decompose the deformation into elastic and plastic parts, which allows a relatively easy calibration of the material parameters involved. The hypoplastic constitutive model captures the extended theory of "critical state soil mechanics" and describes the influence of pressure and density on the incremental stiffness, peak friction angle and dilatancy angle using only eight material parameters. It is also outlined in detail how the compression law by Bauer can be embedded into the hypoplastic model with help of a consistency condition.

In Section 4 the hypoplastic constitutive model shown in Section 3 is extended to describe also time dependent material properties which are relevant for weathered and moisture sensitive rockfill materials. In addition to the current void ratio and stress, the solid hardness and its rate are also state quantities of the extended model. As a consequence creep and stress relaxation properties are usually coupled and the incremental stiffness, peak friction angle, dilatancy angle are also influenced by the evolution of the degradation of the solid hardness.

In Section 5 the capability of the proposed hypoplastic model to model the mechanical behavior of rockfill materials under dry and wet conditions are verified by comparison of numerical simulations with experimental results. In order to simulation sudden changes of the creep velocity initiated by repeated acceleration of the degradation of the solid hardness during the lifetime of the dam an extended version for the evolution equation of the solid hardness is proposed. The enhanced version permits the simulation of multistep degradation of the solid hardness and a refined simulation of collapse settlements and long-time creep.

Throughout the paper the sign convention of rational solid mechanics is adopted, i.e. compressive stresses and strains, and their rates are negative. Indices on vector and tensor components refer to an orthonormal Cartesian basis and the symbol δ_{ij} denotes the Kronecker delta. The summation convention by Einstein over repeated indices is employed. A superimposed dot indicates the material time derivative, e.g. $\dot{e} = \mathrm{d}e/\mathrm{d}t$. All stresses are effective stresses. Other effects of partly saturated materials such as inter-particle capillary forces are negligible for coarse grained rockfill materials.

2. Compression law by Bauer

This section deals with the modeling of essential mechanical properties of weathered and moisture sensitive rockfill materials under isotropic and oedometric compression. To this end the so-called "solid hardness" is defined in the sense of a continuum description and it is a state parameter in the compression law by Bauer. An evolution equation for the degradation of the solid hardness of the rockfill material is used to model the influence of the reduction of the incremental stiffness caused by progressive weathering, instantaneous wetting deformation and long-time creep. Examples for the adaptation of the velocity parameter in the evolution equation of the solid hardness to experimental creep and stress relaxation curves are outlined in detail.

2.1 Introduction of the solid hardness in the sense of a continuum description

Isotropic or oedometric compression tests carried out with various granular materials show qualitatively similar compression curves. At lower stresses the reduction of the void ratio is explained by sliding of neighboring grains against each other and a reorientation of the grain skeleton into a denser state. Under higher pressures the additional compaction is mainly related to progressive grain crushing. In a semi-logarithmic representation, the compression curves show an S-shape which is also clearly visible from the experimental data for two different sand materials in **Figure 2** [70]. For different initial void ratios, the distance between the compression curves becomes smaller with an increase in the mean pressure and for higher pressures the curves merge together. This means that the memory of the material on the initial density fades out due to both grain crushing and reorientation of grains. It is known from experiments that the point of inflection is related to the pressure level where grain crushing becomes dominant. Such a compression behavior was also observed for arbitrary granular materials and it is also verified by

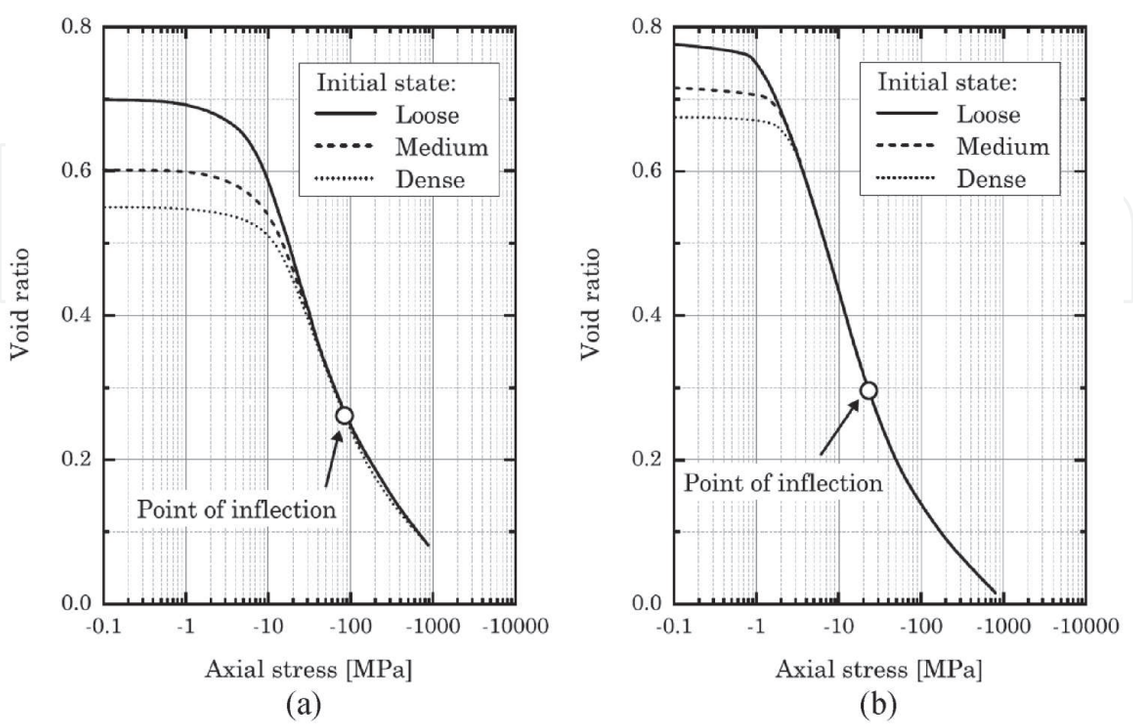

Figure 2.
Decrease of the void ratio with an increase of the axial stress in oedeometer tests on sand specimens starting from different initial void ratios [70]: (a) Cambra sand; (b) Gypsum sand.

numerical simulations with the discrete element method, e.g. [71, 72]. Experimental work has shown that the pressure at the point of inflection depends mainly on the mineral composition and the state of weathering of the solid material. As the point of inflection shows no noticeable influence on the initial density, it is a well-defined state of the material under compression. The pressure where the point of inflection appears is in the following called "solid hardness" and it is a material parameter in the compression law by Bauer [57, 58]. In this context it is worth noting that the solid hardness is defined for the compression behavior of an assembly of grains and does not mean the hardness of a single grain.

In the case of frequently used constitutive models the compression behavior represented in a semi-logarithmic representation is approximated by a straight line as illustrated in **Figure 3a**. However, the approximation is only applicable to a limited pressure range. For higher pressures the compression line, NCL, leads to the non-physical area of negative void ratios. A behavior of this kind cannot occur when using the compression law proposed by Bauer [57, 58]. The exponential function captures the whole pressure range in a consistent manner as depict in **Figure 3b**. In particular, Bauer's isotropic compression law describes the reduction of the void ratio e with an increasing mean effective pressure $p = -(\sigma_{11} + \sigma_{22} + \sigma_{33})/3$ according to the following exponential function:

$$e_i = e_{i0} \exp\left\{-\left(\frac{3p}{h_s}\right)^n\right\}. \tag{1}$$

Eq.(1) represents the upper bound of the pressure dependent maximum void ratio e_i and involves three material parameters. In particular, e_{i0} denotes the maximum void ratio at the initially nearly stress free state, the solid hardness h_s is the value of $3p$ where the compression curve in a semi-logarithmic representation shows the point of inflection, and n is related to the inclination of the compression curve in the point of inflection. The compression law is consistent within the whole pressure range and thus it also takes into account the influence of grain crushing at higher pressures [67].

For rockfill materials the value of the solid hardness is rather high, and usually it cannot be achieved with standard isotropic compression apparatus available in a soil mechanics laboratory. On the other hand, in an oedometer device higher pressures are easier to carry out. Investigations show that for practical application the solid hardness can also be calibrated with sufficient accuracy if data are used which are

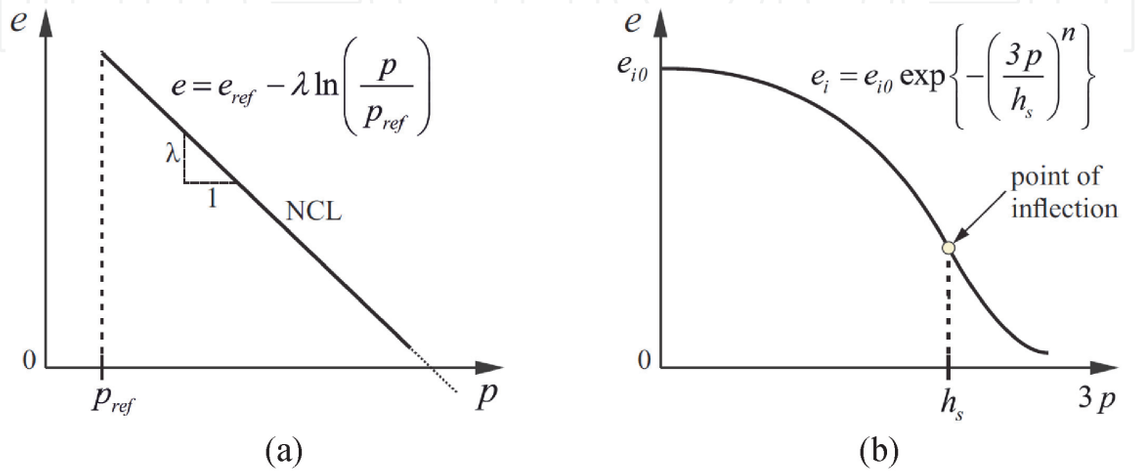

Figure 3.
Illustration of compression laws in the semi-logarithmic representation $e - \ln(3p)$: (a) normal compression line (NCL); (b) compression law by Bauer [58].

obtained from an oedometer test instead of an isotropic test. Standard oedoemeter devices usually only allow the measuring of the vertical stress σ_V, so that the lateral stress $\sigma_H = K_0\sigma_V$ must be estimated for instance with the help of the Jaky formula [73], i.e. for the coefficient of the earth pressure at rest $K_0 \approx 1 - \sin\varphi_c$. Herein φ_c denotes the critical friction angle. Then the mean pressure can be calculated form $p = -\sigma_V(1 + 2K_0)/3$.

The embedding of the compression law (1) into general 3-D constitutive models can be accomplished with the help of a consistency condition. As a heuristic example the embedding into an elastic material model is demonstrated in Appendix A. The implementation of Eq.(1) into an enhanced constitutive model for rockfill materials is discussed in Section 3 and outlined in detail in Appendix B.

2.2 Time dependent process of degradation of the solid hardness

The degradation of the solid hardness caused by progressive weathering of the rockfill material is a time dependent process and causes a reduction of resistance of the material against shearing and compaction. A chemical reaction of the weathered rockfill material with water can accelerate the process of weathering leading to grain breakage and as a consequence to collapse settlements and creep deformations. Experimental investigations show that the solid hardness of the dry material is higher than the solid hardness of the wet material, and that the transition from the dry to the wet state is a time dependent process as illustrated in **Figure 4**.

In order to take the current state of weathering into account, the constant solid hardness h_s in Eq.(1) is replaced by the state quantity h_{st}, i.e.

$$e_i(p,\ \ h_{st}) = e_{i0}\exp\left\{-\left(\frac{3p}{h_{st}}\right)^n\right\}. \tag{2}$$

The change of the void ratio with time t, i.e. $\mathrm{d}e/\mathrm{d}t = \dot{e} < 0$, then depends on the current state of e, p, h_{st}, and the rate quantities $\dot{p}$ and $\dot{h}_{st}$, i.e.

$$\dot{e}\left(e,\ \ p,\ \ h_{st},\ \ \dot{p},\ \ \dot{h}_{st}\right) = n\,e\left(\frac{3p}{h_{st}}\right)^n\left(\frac{\dot{h}_{st}}{h_{st}} - \frac{\dot{p}}{p}\right). \tag{3}$$

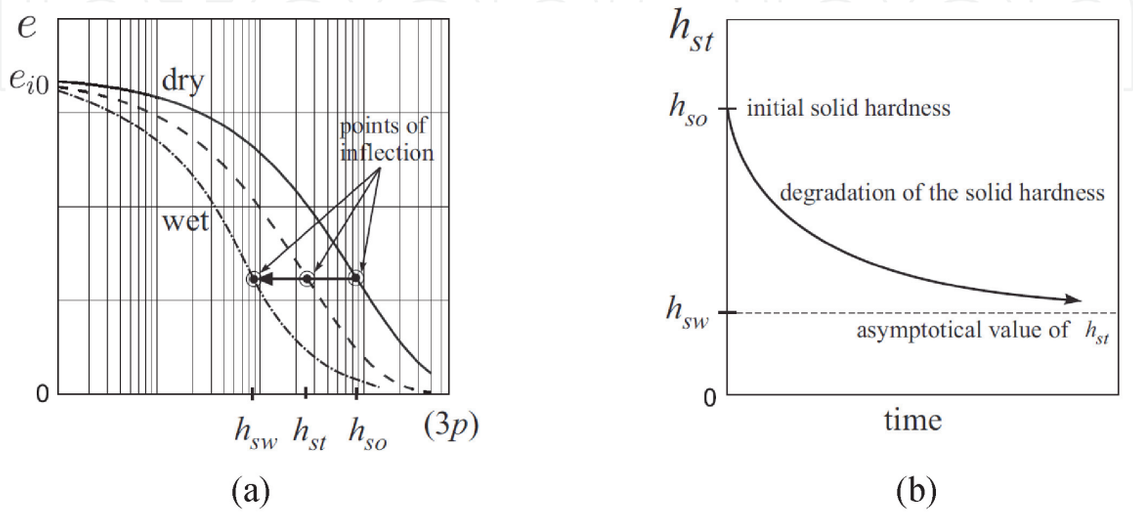

Figure 4.
(a) Transition of the compression curve from the dry to the wet state; (b) time dependent degradation of the solid hardness.

Substituting the identity $\dot{e} = (1+e)\,\dot{\varepsilon}_V$ into Eq.(3) the following relation for the volume strain rate $\dot{\varepsilon}_V$ is obtained:

$$\dot{\varepsilon}_V = \frac{n\,e}{1+e}\left(\frac{3p}{h_{st}}\right)^n\left(\frac{\dot{h}_{st}}{h_{st}} - \frac{\dot{p}}{p}\right). \tag{4}$$

The evolution Eqs. (3) and (4) describe creep and stress relaxation in a unified manner. In particular, for the special case that during degradation of the solid hardness the pressure is kept constant, i.e. $\dot{p} = 0$, the evolution equation for creep can be obtained. For instance, under the constant isotropic stress p_o the evolution equation for the volume strain and for the corresponding void ratio reads:

$$\dot{\varepsilon}_V = \frac{n\,e}{1+e}\left(\frac{3p_o}{h_{st}}\right)^n\left(\frac{\dot{h}_{st}}{h_{st}}\right), \tag{5}$$

and

$$\dot{e} = n\,e\left(\frac{3p_o}{h_{st}}\right)^n\left(\frac{\dot{h}_{st}}{h_{st}}\right), \tag{6}$$

respectively. With respect to the state quantities at the reference time $t = 0$, i.e. $e(t=0) = e_0$ and $h_{st}(t=0) = h_{so}$, the integration of Eq.(6) leads to:

$$e(t) = e_o \exp\left\{\left(\frac{3p_o}{h_{so}}\right)^n - \left(\frac{3p_o}{h_{st}(t)}\right)^n\right\}. \tag{7}$$

The integration of the identity $\dot{e} = (1+e)\,\dot{\varepsilon}_V$ with respect to $\varepsilon_V(t=0) = 0$ and $e(t=0) = e_0$ leads to:

$$e(t) = (1+e_0)\exp\{\varepsilon_V\} - 1. \tag{8}$$

The comparison of Eq.(7) with Eq.(8) yields the creep strain ε_V depending on the current state of the solid hardness h_{st}:

$$\varepsilon_V(t) = \ln\left[\frac{e_0 \exp\left\{\left(3p_o/h_{so}\right)^n - \left(3p_o/h_{st}(t)\right)^n\right\} + 1}{(1+e_0)}\right]. \tag{9}$$

On the other hand for the special case that the volume is kept constant, i.e. $\dot{\varepsilon}_V = 0$, Eq.(4) leads the evolution equation for stress relaxation:

$$\dot{p} = p\left(\frac{\dot{h}_{st}}{h_{st}}\right). \tag{10}$$

With respect to $p(t=0) = p_o$ and $h_{st}(t=0) = h_{so}$ the integration of Eq.(10) leads the stress relaxation law:

$$p(t) = \frac{p_o}{h_{so}}\,h_{st}(t). \tag{11}$$

For the irreversible degradation of the solid hardness with time, i.e. $\mathrm{d}h_{st}/\mathrm{d}t = \dot{h}_{st} < 0$, an appropriate constitutive relation must be chosen. The constitutive

function should capture the influence of the essential state quantities relevant for the complex chemical and mechanical response of the stressed material under different environmental events, such as the repeated change of the moisture content caused by rain water infiltration into the dam body. On the other hand, the evolution equation should allow an easy calibration based on the available experimental data. Thus, a compromise must usually be found for practical applications. In this paper the following phenomenological evolution equation based on data from creep tests or stress relaxation tests is considered [67]:

$$\dot{h}_{st} = -\frac{1}{c}(h_{st} - h_{sw}), \tag{12}$$

where parameter c has the dimension of time and parameter h_{sw} denotes the final value of the degraded solid hardness. The integration of Eq.(12) yields for the solid hardness depending on the time t:

$$h_{st}(t) = h_{sw} + (h_{so} - h_{sw}) \exp\left\{-\frac{t}{c}\right\}, \tag{13}$$

where parameter h_{so} denotes the value of the solid hardness at the reference time $t = 0$ and it can be obtained by adaptation of Eq.(1) to the compression curve of the material in the dry state. Moisture sensitive and weathered rockfill materials usually exhibits a higher compressibility and thus the solid hardness is lower than for the dry material. The value of parameter h_{sw} denotes the asymptotic value for $t \to \infty$ and can be adapted to the compression curve for the material under wet condition. The degraded solid hardness, h_{sw}, takes into account contributions of both creep deformations and collapse settlements. For a refined modeling the evolution equation for the degradation can be extended to distinguish collapse deformation and long-term deformation as demonstrated in Section 5. Parameter c has the dimension of time and can be calibrated from the volume creep curve or from the stress relaxation test as outlined in Appendix B. When experimental data are only available for creep curves under deviatoric stresses the mechanical response is also affected by the current packing density and stress deviator so that parameter h_{sw} and c must be calibrated using the coupled constitutive model outlined in Section 4. It is also worth noting that parameter h_{sw} and c are usually not material constants and may change as a consequence of repeated changes of environmental conditions during the whole lifetime of the dam as also discussed in Section 5.2.

Weathered rockfill materials can also undergo creep deformation and stress relaxation under dry condition and it can be distinguished between instantaneous deformation and time dependent deformation. The time dependent compressibility of the dry material can be explained by delayed grain crushing and it can also be modeled by a degradation of the solid hardness. In this case h_{sw} in Eq.(12) denotes the asymptotical value of h_{st} related to the dry state of the material.

The value of parameter h_{sw} can also be back calculated from the asymptotic value of the creep curve or stress relaxation curve. In particular, the asymptotic value of the volume strain can be estimated form the creep curve, i.e. $\varepsilon_{V\infty} = \varepsilon_V(t \to \infty)$, so that the quantity of $h_{sw} = h_{st}(t \to \infty)$ can be calculate from Eq.(9) for $t \to \infty$, i.e.

$$h_{sw} = 3p_o \left[\left(\frac{3p_o}{h_{so}} \right)^n - \ln \left[\frac{(1+e_0)}{e_0} \exp\{\varepsilon_{V\infty}\} - 1 \right] \right]^{(-1/n)}. \tag{14}$$

From a pure stress relaxation test the value of h_{sw} can also be calculated from Eq.(11) to:

$$h_{sw} = h_{so}\frac{p_\infty}{p_o}, \tag{15}$$

where $p_\infty = p(t \to \infty)$ denotes value of the mean stress at the end of stress relaxation. The value can be estimated from the asymptote of the stress relaxation curve.

3. Embedding the solid hardness into hypoplasticity

To demonstrate the embedding of the solid hardness h_o into a 3-D constitutive model the hypoplastic model for cohesionless soil proposed by Gudehus [69] and Bauer [58] is considered in the following. In particular, the components of the objective stress tensor for the general form of the nonlinear constitutive equation reads:

$$\sigma_{ij}^{\nabla} = f_s\left[\hat{a}^2\dot{\varepsilon}_{ij} + (\hat{\sigma}_{kl}\,\dot{\varepsilon}_{kl})\,\hat{\sigma}_{ij} + f_d\,\hat{a}\left(\hat{\sigma}_{ij} + \hat{\sigma}_{ij}^*\right)\sqrt{\dot{\varepsilon}_{kl}\,\dot{\varepsilon}_{kl}}\right]. \tag{16}$$

The quantities in Eq.(16) denote:
σ_{ij}^{∇} ... objective stress rate
$\dot{\varepsilon}_{ij}$ ... strain rate
σ_{ij} ... effective Cauchy stress
$\hat{\sigma}_{ij}$ ... normalized effective Cauchy stress, i.e. $\hat{\sigma}_{ij} = \sigma_{ij}/\sigma_{kk}$
$\hat{\sigma}_{ij}^*$ ... deviatoric part of $\hat{\sigma}_{ij}$, i.e. $\hat{\sigma}_{ij}^* = \hat{\sigma}_{ij} - \delta_{ij}/3$
$\hat{a}$ ... critical stress factor
f_s ... stiffness factor
f_d ... relative density factor

Because of the nonlinearity of $\sqrt{\dot{\varepsilon}_{kl}\,\dot{\varepsilon}_{kl}}$ the hypoplastic constitutive Eq.(1) is apt to models irreversible deformations without any decomposition of the deformation into elastic and plastic parts. Factor $\hat{a}$ is a function of the critical friction angle, φ_c, and the invariants of the stress deviator. The adaptation of $\hat{a}$ to the stress limit condition by Matsuoka and Nakai [74] is illustrated in **Figure 5a** and represented in the hypoplastic model as [67]:

$$\hat{a} = \frac{\sin\varphi_c}{3 - \sin\varphi_c}\left[\sqrt{\frac{8 - 9\left(\hat{\sigma}_{pq}^*\,\hat{\sigma}_{pq}^* + \hat{\sigma}_{kl}^*\,\hat{\sigma}_{lm}^*\,\hat{\sigma}_{mk}^*\right)}{3 - 9\left(\hat{\sigma}_{kl}^*\,\hat{\sigma}_{lm}^*\,\hat{\sigma}_{mk}^*\right)/\left(\hat{\sigma}_{pq}^*\,\hat{\sigma}_{pq}^*\right)}} - \sqrt{\hat{\sigma}_{kl}^*\,\hat{\sigma}_{kl}^*}\right]. \tag{17}$$

The peak friction angle and dilatancy are predictions of the constitutive Eq. (16) and not material constants. The influence of pressure and density on the peak friction angle and dilatancy angle is modeled using the pressure dependent relative density factor f_d, which represents a relation between the current void ratio e, the critical void ratio, e_c and the minimum one e_d, i.e.

$$f_d = \left(\frac{e - e_d}{e_c - e_d}\right)^{\alpha}, \tag{18}$$

where α is a material parameter. The change of the volume of the rockfill material is related to a change of the void ratio which can be expressed by the following evolution equation:

$$\dot{e} = (1+e)\dot{\varepsilon}_V. \tag{19}$$

In Eq.(18) the pressure dependent quantities e_c and e_d can be related to the compression law (1) according to the postulate by Gudehus [69], i.e.:

$$\frac{e_c}{e_{c0}} = \frac{e_d}{e_{d0}} = \frac{e_i}{e_{i0}} = \exp\left\{-\left(\frac{3p}{h_s}\right)^n\right\}, \tag{20}$$

where e_{c0}, e_{d0} and e_{i0} are the values for $p \simeq 0$. Eq.(20) describes a reduction of the limit void ratios and the critical void ratio with increasing mean stress as illustrated in **Figure 5b**.

The influence of the pressure and density on the incremental stiffness is modeled using the stiffness factor f_s, which can be represented as the product of three parts, i.e.:

$$f_s = f_e f_\sigma f_b. \tag{21}$$

The first term on the right hand side of Eq.(21) is the density dependent part and a relation between the pressure dependent maximum void ratio e_i and the current void ratio e, i.e.:

$$f_e = \left(\frac{e_i}{e}\right)^\beta, \tag{22}$$

where β is a material parameter. Factor f_σ takes into account a decrease in the incremental stiffness with an increase of $\hat{\sigma}_{kl}\hat{\sigma}_{kl}$, i.e.:

$$f_\sigma = \frac{1}{\hat{\sigma}_{kl}\hat{\sigma}_{kl}}. \tag{23}$$

Factor f_b is referred to as the barotropy factor and is obtained by a consistency condition, which allows the embedding of the compression law by Bauer into the hypoplastic constitutive Equation [67, 69]. In particular, for monotonic isotropic

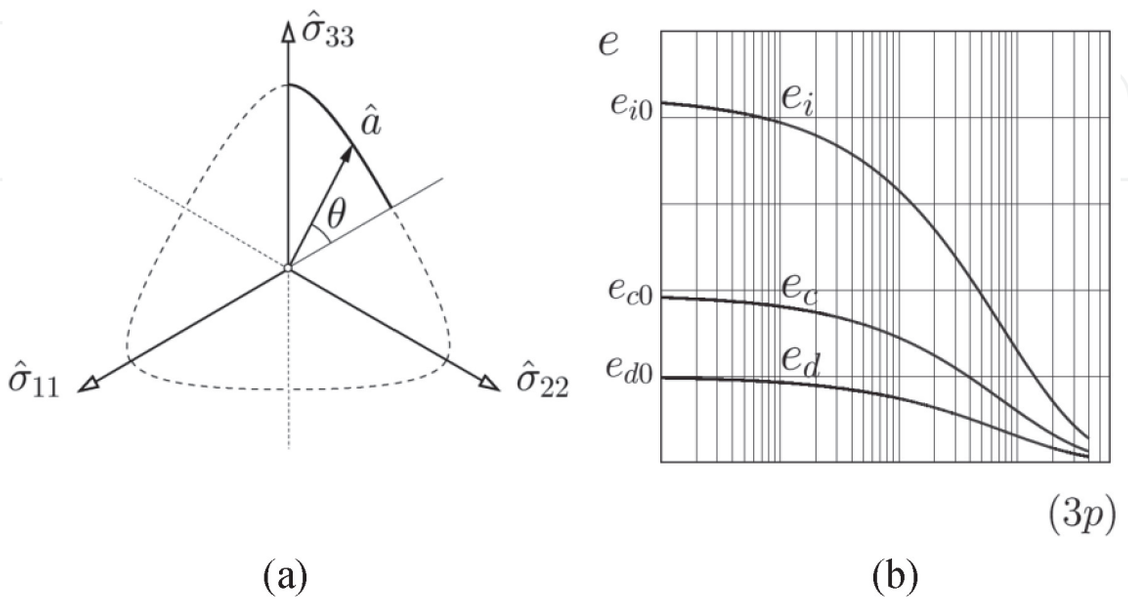

Figure 5.
(a) Stress limit condition by Matsuoka and Nakai [74] in the deviator plane; (b) pressure dependence of the maximum void ratio e_i, critical void ratio e_c and minimum void ratio e_d in the phase diagram of void ratios.

compression the rates of the mean stresses obtained from the compression law (1) and the hypoplastic constitutive Eq. (16) must coincide. The detailed derivation of the consistency condition is outlined in Appendix C. For factor f_b one obtains:

$$f_b = \frac{h_s\,(1+e_i)}{n\,e_i}\quad\left[\frac{8\,\sin^2\varphi}{(3-\,\sin\varphi)^2}+1-\frac{2\sqrt{2}\sin\varphi}{(3-\,\sin\varphi)}\left(\frac{e_{i0}-e_{d0}}{e_{c0}-e_{d0}}\right)^{\alpha}\right]^{-1}\left(\frac{3p}{h_s}\right)^{(1-n)}. \tag{24}$$

The hypoplastic constitutive model also captures properties according to the theory of the "critical state soil mechanics" [75]. In particular, in critical states the pressure dependent void ratio $e = e_c$ and thus, factor $f_d = 1$. By applying the condition that in critical states the stress rate and volume strain rate must simultaneously vanishing under continuous deformation, i.e. $\boldsymbol{\sigma}^{\nabla} = \mathbf{0}$, $\dot{\varepsilon}_V = 0$ and $\dot{\boldsymbol{\varepsilon}} \neq \mathbf{0}$, to Eq.(16) one obtains: $\hat{a}^c = \|\hat{\boldsymbol{\sigma}}^{*c}\| = \sqrt{\hat{\sigma}^{*c}_{kl}\,\hat{\sigma}^{*c}_{kl}}$. Herein $\hat{a}^c$ is the corresponding value of $\hat{a}$ obtained from Eq.(17) and $\|\hat{\boldsymbol{\sigma}}^{*c}\|$ denotes the norm of the normalized deviatoric stress tensor in the critical state [76]. With respect to the critical friction angle φ_c, which is defined for the critical state reached under monotonic triaxial compression, factor $\hat{a}^c$ takes the value: $\hat{a}^c = \sqrt{8/3}\,\sin\varphi_c/(3-\,\sin\varphi_c)$.

The hypoplastic constitutive Eq. (16) contains eight material parameters, i.e. $\varphi_c, h_s, n, e_{io}, e_{co}, e_{do}, \alpha, \beta$, which can be calibrated from standard laboratory tests as outlined in [58]. The capacity of the model in simulating the essential features of an initially loose and dense state of the soil using the same set of material parameters is demonstrated for instance in [58].

4. Extension of the hypoplastic model to weathered and moisture sensitive rockfill materials

Although the hypoplastic constitutive Eq. (16) is of the rate type, the material behavior described is rate independent. In order to take into account rheological properties of weathered and moisture sensitive rockfill materials in the hypoplastic model outlined in the previous section the constant solid hardness h_s is replaced with a state dependent solid hardness $h_{st}(t)$. Furthermore, an additional term is added in the extended hypoplastic model to capture the influence of the rate of the solid hardness, $\dot{h}_{st}(t)$, on the mechanical response. The extended hypoplastic constitutive equation reads [47]:

$$\sigma^{\nabla}_{ij} = f_s\left[\hat{a}^2\dot{\varepsilon}_{ij} + (\hat{\sigma}_{kl}\,\dot{\varepsilon}_{kl})\,\hat{\sigma}_{ij} + f_d\,\hat{a}\left(\hat{\sigma}_{ij}+\hat{\sigma}^*_{ij}\right)\sqrt{\dot{\varepsilon}_{kl}\,\dot{\varepsilon}_{kl}}\right] + \frac{\dot{h}_{st}}{h_{st}}\left[\frac{1}{3}\sigma_{kk}\,\delta_{ij} + \kappa\sigma^*_{ij}\right]. \tag{25}$$

In Eq.(25) the degradation of the solid hardness is coupled with the evolution of stress and strain. As the pressure dependent limit void ratios defined in Eq.(20) are also functions of the current state of the solid hardness a degradation of the solid hardness also results in a reduction of the limit void ratios. For a lower solid hardness the stiffness factor f_s and density factor f_d are also lower, so that the incremental stiffness and the peak friction angle predicted with the constitutive Eq. (25) are also lower. In the last term on the right hand side of Eq.(25) parameter κ scales the effect of the stress deviator on stress relaxation and creep. Numerical studies in [53, 48, 49] show that parameter κ of Eq.(25) has a significant influence on the inclination of the volume creep path $\mathrm{d}\varepsilon_V/\mathrm{d}\varepsilon_{11}$. The calibration of parameter κ is discussed in Section 5.

For general boundary conditions the evolution of creep is obtained for $\sigma_{ij}^{\nabla} = 0$, i.e.:

$$f_s \left[\hat{a}^2 \dot{\varepsilon}_{ij} + (\hat{\sigma}_{kl}\, \dot{\varepsilon}_{kl})\, \hat{\sigma}_{ij} + f_d\, \hat{a} \left(\hat{\sigma}_{ij} + \hat{\sigma}_{ij}^{*} \right) \sqrt{\dot{\varepsilon}_{kl}\, \dot{\varepsilon}_{kl}} \right] + \frac{\dot{h}_{st}}{h_{st}} \left[\frac{1}{3} \sigma_{kk}\, \delta_{ij} + \kappa \sigma_{ij}^{*} \right] = 0, \quad (26)$$

and for pure stress relaxation, i.e. stress changes under $\dot{\varepsilon}_{ij} = 0$, the constitutive Eq. (25) reduced to:

$$\sigma_{ij}^{\nabla} = \frac{\dot{h}_{st}}{h_{st}} \left[\frac{1}{3} \sigma_{kk}\, \delta_{ij} + \kappa \sigma_{ij}^{*} \right]. \quad (27)$$

For the special case of isotropic stress states under $e = e_i$ Eq. (26) turns into the creep law (5) and Eq. (27) ends up with the evolution law (10) for stress relaxation. Parameters c and h_{sw} involved in the evolution Eq. (12) can be calibrated from isotropic compression tests as outlined in Appendix B. It should be noted that a decoupling of creep and stress relaxation is only possible under special boundary conditions. In general boundary value problems creep and stress relaxation are usually coupled. Time dependent deformations and local stress rearrangements can then interact each other, so that in such cases the coupled constitutive Eq. (25) needs to be applied. When the degradation of the solid hardness has been completed, i.e. the final value h_{sw} of the solid hardness is reached, the constitutive Eq. (25) turns into the constitutive Eq. (16).

5. Numerical simulations

In the following the performance of the proposed constitutive concept for modeling the degradation of the solid hardness is demonstrated by comparing experimental data with the results of numerical simulations of a multistep, one dimensional creep test, and triaxial creep tests under different deviatoric stresses. For numerical modeling of wetting induced settlements a smooth transition from an almost sudden settlement, i.e. collapse settlement, to the creep deformation is assumed. A smooth transition of the kind is also observed in laboratory experiments and can be modeled with an extended evolution equation of the solid hardness as demonstrated in the following.

5.1 Combined modeling of collapse deformation and creep

In this subsection the results of wetting experiments with broken sandstone carried out by Fu et al. [77] are considered for the simulation with a simplified version of the hypoplastic constitutive model proposed in [60], which differs from the hypoplastic model (25) in that for the density factor the simplified relation $f_d = (e/e_c)^{\alpha}$, for $\beta = 1$, and for the critical void ratio curve the relation $e_c = e_{co} \exp\{-(3p/73.5)^n\}$ is used. In the experiments the initially dry specimen was loaded up to a certain stress ratio and then wetted under the constant stress. For the dry state of the material the material parameters were calibrated based on the assumption of a constant solid hardness. The detailed calibration procedure applied is outlined in [60]. The values for the material parameters obtained are: $\varphi_c = 40^{\circ}$, $h_{so} = 120$ [MPa], $n = 0.82$, $e_{io} = 0.3$, $e_{co} = 0.24$ and $\alpha = 0.18$. For the modeling of the time dependent process of degradation of the solid hardness caused by wetting the following additional material parameters were obtained:

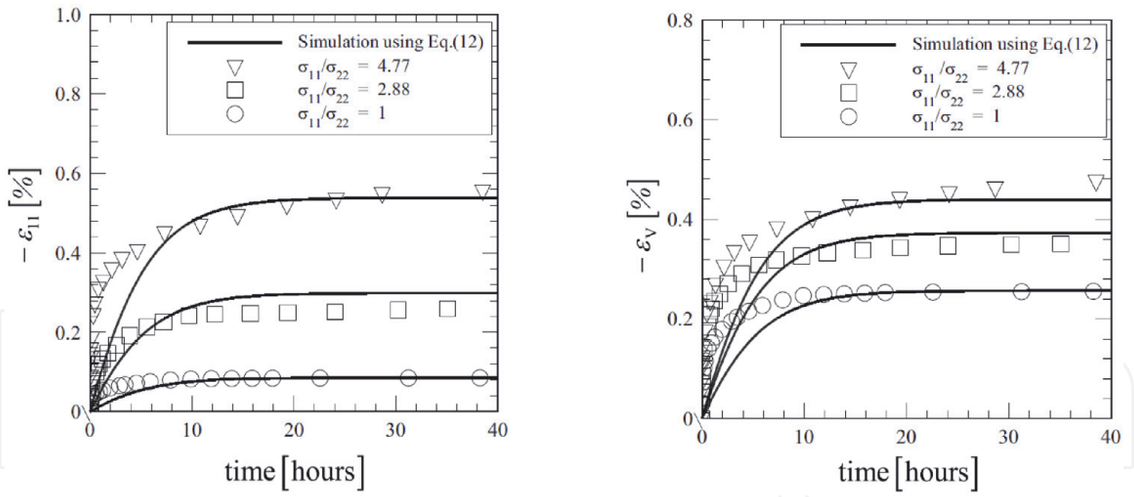

Figure 6.
Creep curves under a confining stress of $\sigma_{22} = -1200$ [kPa] and different stress ratios; the shapes indicate experimental data by Fu et al. [77]; solid curves are the numerical results obtained with respect to Eq.(13) for the degradation of the solid hardness.

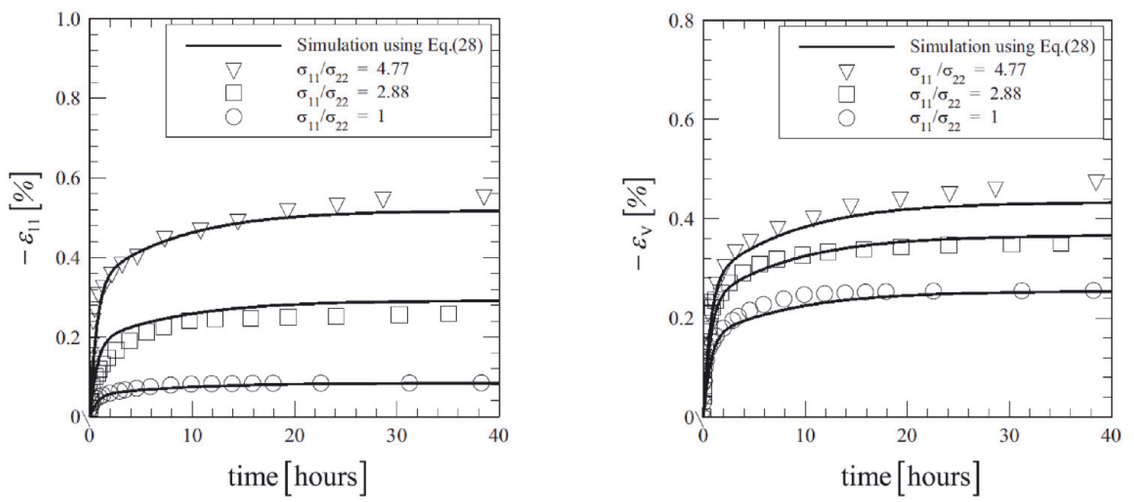

Figure 7.
Creep curves under a confining stress of $\sigma_{22} = -1200$ [kPa] and different stress ratios; the shapes indicate experimental data by Fu et al. [77]; solid curves are the numerical results obtained with respect to the extended Eq.(28) for the degradation of the solid hardness.

$$h_{sw} = 78.5 \text{ [MPa]}; c = 4.0 \text{ [h]}; \kappa = 0.6.$$

Numerical investigation with respect to the constitutive relation (13) show [60], that the prediction of the time dependent deformations immediately after wetting deviates from the experimental data. In particular, at initiation of creep the axial creep strain ε_{11} and the volume creep strain ε_V are underestimated as shown for a confining strass of $\sigma_{22} = -1200$ [kPa] and at three different stress ratios in **Figure 6**. It is obvious that the three material parameters h_{so}, h_{sw} and c of the constitutive relation (13) are not sufficient to capture both collapse settlements and long-time creep. For a refined modeling of wetting induced deformations the evolution Eq. (12) for the degradation of the solid hardness is extended and formulated as the sum of two parts [51], i.e.

$$\dot{h}_{st} = \dot{h}_{st\ \ collapse} + \dot{h}_{st\ \ creep}. \tag{28}$$

Herein $\dot{h}_{st\ \ collapse} = -\left(h_{st\ \ collapse} - h_{sw\ \ collapse}\right)/c_1$ denotes the part of the degradation of the solid hardness related to collapse deformation and

$\dot{h}_{st\ \ creep} = -\left(h_{st\ \ creep} - h_{sw\ \ creep}\right)/c_2$ is the part related to long-term creep. As no clear distinction between collapse settlements and long-term creep can be detected from experiments, the constitutive parameters $c_1 < c_2$ and $h_{sw\ \ collapse} > h_{sw\ \ creep}$ can be calibrated using an optimization procedure. For consistency the difference of $h_{sw\ \ collapse}$ and $h_{sw\ \ creep}$ must be the same as the asymptotical value h_{sw} obtained with the constitutive Eq. (12), i.e. $h_{sw\ \ collapse} - h_{sw\ \ creep} = h_{sw}$. The quantities $1/c_1$ and $1/c_2$ control the velocities of the degradation of the solid hardnesses $h_{sw\ \ collapse}$ and $h_{sw\ \ creep}$, respectively. Thus, the quantity $1/c_1$ is related to the deformation velocity immediately after wetting, while the quantity $1/c_2$ is relevant of the long term creep. The values c_1 and c_2 can be optimized with respect to the experimental creep curve. The procedure leads for the evolution Eq. (28) the following material parameters:

$h_{sw\ \ collapse}$ = 90.5 [MPa]; c_1 = 0.6 [h]; $h_{sw\ \ creep}$ = 12.0 [MPa] and c_2 = 8.0 [h].

The results of numerical simulations using the extended evolution Eq. (28) are in good agreement with the experimental results as shown for the axial strain ε_{11} and volume strain ε_V in **Figure 7**.

5.2 Multistep creep

In order to simulation multistep creep initiated by repeated acceleration in the degradation of the solid hardness, e.g. caused by repeated rain water infiltration events into the rockfill body of the dam, two different concepts can be suggested for practical application. Either each event is modeled independent of the previous one, i.e. the values for parameters c and h_{sw} are calibrated for each individual creep curve, or subsequent events are modeled with respect of ongoing contributions of previous events. For the latter the rate of the solid hardness, $\dot{h}_{st\,(i)}$, of event (i) can be represented as:

$$\dot{h}_{st\,(i)} = \dot{h}_{st(i)collapse} + \sum_{k=1}^{i-1} \dot{h}_{st\,(k)}. \tag{29}$$

In Eq.(29) the terms on the right hand side consist of the contribution $\dot{h}_{st\,(i)collapse}$ initiated by a rapid change of the solid hardness in event (i), and the sum of contributions $\dot{h}_{st\,(k)}$ of previous events. Numerical simulations show that the accumulation concept proposed in Eq.(29) allows a more refined modeling of the whole history of creep and stress relaxation [51]. The application of the accumulation concept is illustrated in **Figure 8** based on the creep experiment by Sowers et al. [3]. To this end three sections can be distinguished. From the experimental data of section I the initially solid hardness h_{so} can be computed from the instantaneous settlement caused by the applied load of -0.8 MPa on the dry specimen. As no complete data for calibration are available the numerical simulations were carried out using an assumed value for the initial void ratio and estimated material parameters obtained by back analysis. In section II the creep deformation of the dry material can be modeled using the evolution Eq. (12) for the degradation of the solid hardness, $\dot{h}_{st\,\mathrm{II}}$. Herein the final value of the degraded solid hardness $h_{sw\,\mathrm{II}}$ can be obtained from Eq.(14) with respect to an estimated asymptotic value of the creep strain $\varepsilon_{V\infty\mathrm{II}}$. The degradation of the solid hardness in section III can be expressed as a combination of the influence of long-term creep in section II and the deformation immediately after flooding the specimen at time $t = 4500$minutes, i.e.

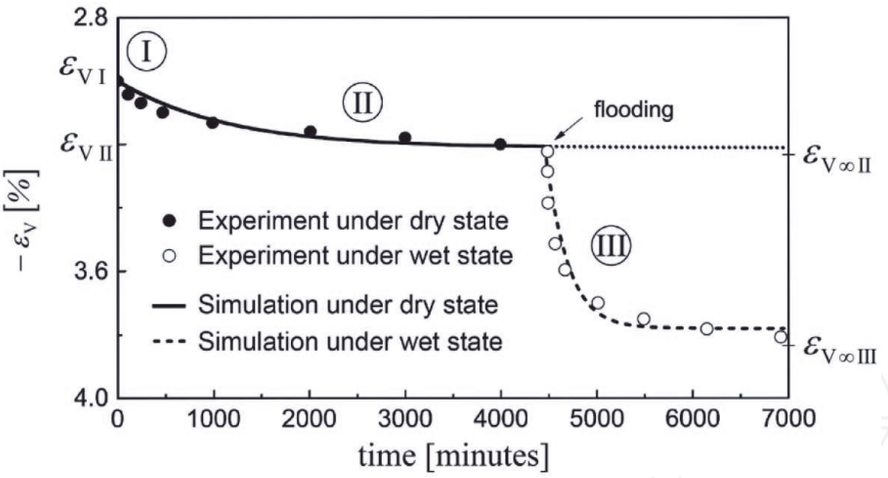

Figure 8.
Creep behavior of the stresses specimen under dry and wet conditions; experiments by Sowers et al. [3].

$\dot{h}_{st\,III} = \dot{h}_{st\,III\,collapse} + \dot{h}_{st\,II}$. The value of $h_{sw\,III}$ can be calculated from an estimation of the asymptotic value $\varepsilon_{V\infty III}$. The creep velocities in part II and part III are different and the corresponding parameters c_{II} and c_{III} can be calibrated using Eq.(B5).

5.3 Influence of the stress deviator on the evolution of the creep deformation

The results of numerical simulations of the influence of the deviatoric stress on the stress strain relationship and on the creep behavior for a moisture sensitive broken sandstone are shown together with the experimental data in **Figure 9**. The 11 material parameter of the extended hypoplastic constitutive model were calibrated by

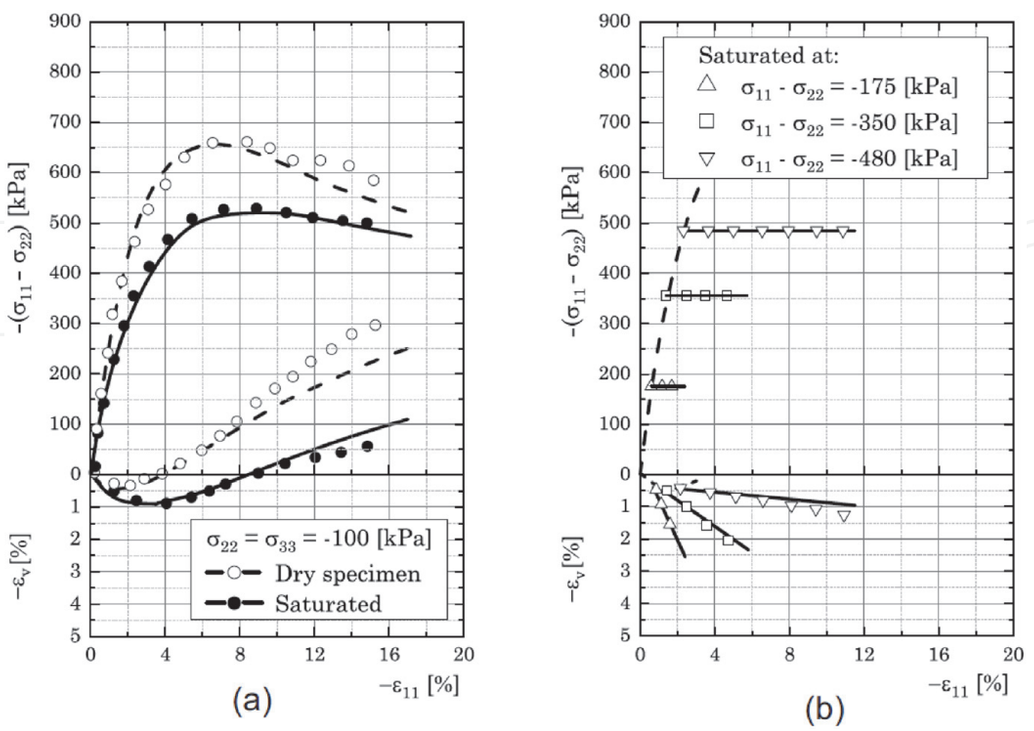

Figure 9.
Response of broken sandstone under triaxial compression: Dashed curves and solid curves are numerical responses for the dry and the water saturated specimens, respectively [50]; shapes denote the experimental data by Li [78].

Bauer et al. [50] using the experimental data obtained by Li [78]. As no creep behavior of the dry material in the triaxial compression test was reported, the calibration of the hypoplastic material parameters for the dry material were carried out for a constant solid hardness. In particular, the following set of material parameters were obtained for the initially dry material: $\varphi_c = 40°$, $h_{so} = 47$[MPa], $n = 0.3$, $e_{io} = 0.59$, $e_{co} = 0.48$, $e_{do} = 0.20$, $\alpha = 0.18$ and $\beta = 2.50$. In the wet state the stressed material showed pronounced rheological behavior, which is taken into account in the numerical simulation by a degradation of the solid hardness using Eq.(13). For the saturated state of the material the additional material parameters for the extended hypoplastic model (25) are: $h_{sw} = 11.5$[MPa], $\kappa = 0.7$ and $c = 3$days.

For monotonic triaxial compression under a lateral stress of $\sigma_{22} = -100$ [kPa] the numerical results are compared with the experimental data in **Figure 9a** for both dry and water saturated state of the material. As can be seen the course of the deviatoric stress $(\sigma_{11} - \sigma_{22})$ and the volumetric strain ε_V against the axial strain ε_{11} is different for the dry and the water saturated materials. The compaction at the beginning of deviatoric loading is higher and the subsequent dilatancy is much lower for the water saturated material. It can therefore be suspected that the critical void ratio will also be lower for the water saturated material. This is well captures with relation (20) for the critical void ratio depending on the mean stress and current state of the degraded solid hardness. The lower peak value of the deviatoric stress $(\sigma_{11} - \sigma_{22})$ and the subsequent strain softening is also well predicted with the same set of material parameters by the hypoplastic constitutive model proposed. In this context it can be noted that the peak value of $(\sigma_{11} - \sigma_{22})$ is not a material constant and is triggered in the extended constitutive Eq. (20) by the pressure dependent relative density factor f_d, which also depends on the current state of the degraded solid hardness h_{st} .

The behavior after water saturation at different deviatoric stresses is shown in **Figure 9b**. It is clearly visible that the axial creep strain ε_{11} is more pronounced for a higher level of the deviatoric stress. The corresponding volumetric creep paths, $\varepsilon_V(\varepsilon_{11})$, are almost linear and in good agreement with the experimental data. The inclination of $\mathrm{d}\varepsilon_V/\mathrm{d}\varepsilon_{11}$ decreases with an increase of the axial strain. The course of the stress ratio σ_{11}/σ_{22} against the inclination of the volumetric creep path, $\mathrm{d}\varepsilon_V/\mathrm{d}\varepsilon_{11}$,

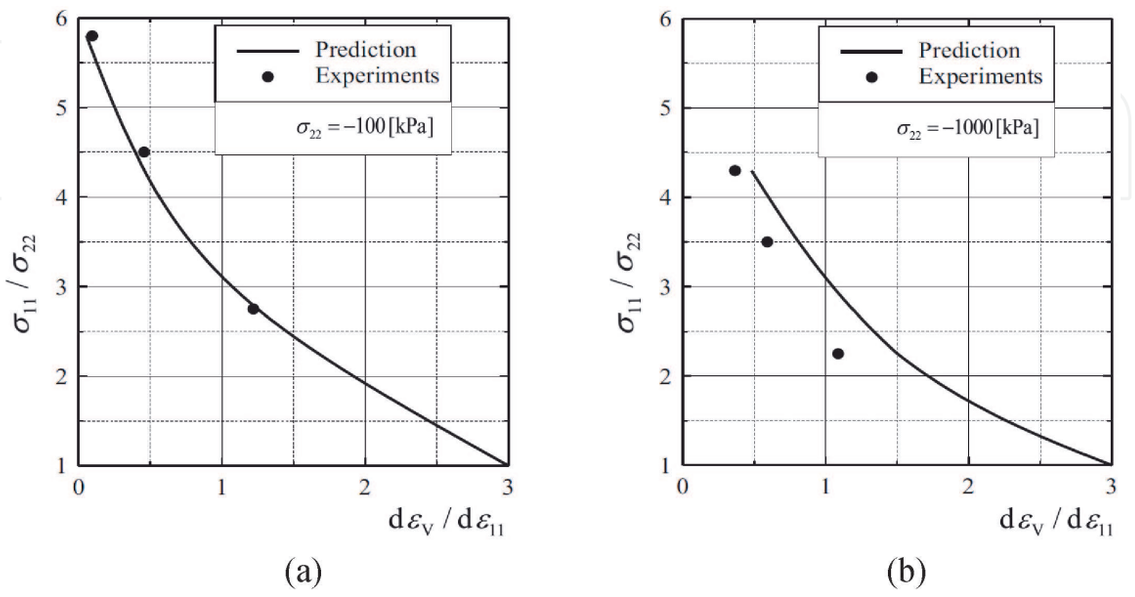

Figure 10.
Influence of the stress ratio σ_{11}/σ_{22} on the inclination of the volume strain curve $\mathrm{d}\varepsilon_V/\mathrm{d}\varepsilon_{11}$ under creep for a lateral stress of: (a) -100 [kPa]; and (b) -1000 [kPa]; the solid curves are numerical results; the shapes indicate experimental data by Li [78].

is nonlinear as shown in **Figure 10a**. With the same set of material parameters numerical simulations are also carried out for a ten times higher lateral stress, i.e. for $\sigma_{22} = -1000$ [kPa]. The corresponding relation between σ_{11}/σ_{22} and $\mathrm{d}\varepsilon_V/\mathrm{d}\varepsilon_{11}$ is shown in **Figure 10b**. Although the trend of the course is similar as for the lower lateral stress, there is a certain deviation between the numerical prediction and the experimental results. Numerical investigations show that the inclination of $\mathrm{d}\varepsilon_V/\mathrm{d}\varepsilon_{11}$ is mainly influenced by parameter κ of Eq.(25). The calibration of parameter κ based on the creep curve for a lower mean stress leads to predicted values of $\mathrm{d}\varepsilon_V/\mathrm{d}\varepsilon_{11}$, which are higher for a higher mean stress, i.e. the deviation to the experimental results increases with an increase of the mean stress. Fu et al. [32] showed that for different mean stresses and different stress ratios the experimental data can be largely approximated using a single hyperbolic function. The numerical simulations with the suggested approximation function, however, still show certain deviations from the experimental data. The investigations indicate that for a refined modeling parameter κ in Eq.(25) should be a function depending on the mean stress and the loading history. An appropriate modeling is still in progress.

6. Conclusions

In this paper the long-term behavior of weathered and moisture sensitive coarse-grained rockfill material is reviewed and the main mechanical properties are modeled in a phenomenological manner using a novel constitutive model based on the frame work of hypoplasticity. In order to take into account of the influence of grain crushing and the time dependent process of degradation of the strength of the solid material on the incremental stiffness, a so-called "solid hardness" is introduced as a state parameter into the constitutive model. The solid hardness is defined for monotonic isotropic compression of a grain assembly and it is a key parameter in the compression law by Bauer. It is shown that creep and stress relaxation are usually coupled. The calibration procedure of the material parameter relevant for the velocity of degradation of the solid hardness is outlined for different states at the creep curve and stress relaxation curve obtained in isotropic compression experiments. It is demonstrated that the strategy used for the embedding of the compression law into an extended 3-D hypoplastic continuum model can also be applied to other classes of constitutive models. With an enhanced hypoplastic constitutive model the influence of the state of weathering, the evolution of the degradation of the solid hardness, the packing density of the rockfill materials and the stress state on the incremental stiffness, the peak friction angle and the dilatancy angle can be modeled in a unified manner using a single set of material parameters. These properties of the model are confirmed by the comparison of numerical simulations with experimental data, in particular for triaxial compression tests under dry and wet conditions as well as for creep tests under different deviatoric stresses. It is shown that the evolution of the volume strain curve under creep strongly depends on the amount of the stress deviator where the rockfill material is saturated. The extended version of the evolution equation for the degradation of the solid hardness permits a refined modeling of collapse settlements and long-time creep caused by repeated changes of environmental conditions.

Acknowledgements

The author wishes to thank Dr. Z.Z. Fu, Dr. L. Li, Mr. M. Khosravi and Mr. S. Safikhani during their stay at the Institute of Applied Mechanics at Graz University of Technology for preparing parts of the numerical simulations shown in this paper.

Appendix A

As a heuristic example for the adaptation of the compression law (1) to a nonlinear elastic material description the following isotropic elastic material law is considered

$$\sigma_{ij} = K\,\varepsilon_{kk}\,\delta_{ij} + 2G\left(\varepsilon_{ij} - \frac{1}{3}\varepsilon_{ll}\delta_{ij}\right). \tag{A1}$$

Herein the bulk modulus, K, and shear modulus, G, are functions of invariants of chosen state variables such as the mean pressure or current void ratio. For isotropic compression Eq.(A1) leads for the mean pressure p:

$$p = -\frac{1}{3}\sigma_{ii} = -K\,\varepsilon_{kk}. \tag{A2}$$

With respect to the relationship $\mathrm{d}e = (1+e)\mathrm{d}\varepsilon_{\mathrm{V}}$ one obtains for the volumetric strain $\varepsilon_{\mathrm{V}} = \varepsilon_{kk}$ as a function of the current void ratio e and the initial void ratio $e_o = e(\,\varepsilon_{\mathrm{V}} = 0;\quad p = 0\,)$:

$$\varepsilon_{\mathrm{V}} = \ln\left(\frac{1+e}{1+e_o}\right). \tag{A3}$$

Substitution of Eq.(A3) into Eq.(A2) leads to:

$$p = -K\,\ln\left(\frac{1+e}{1+e_o}\right) = K\ln\left(\frac{1+e_o}{1+e}\right). \tag{A4}$$

The compression law (1), i.e.

$$e = e_o\exp\left\{-\left(\frac{3p}{h_s}\right)^n\right\}$$

can be transformed to:

$$p = \frac{h_s}{3}\left[\ln\left(\frac{e_o}{e}\right)\right]^{(1/n)}. \tag{A5}$$

The comparison of relation (A4) with relation (A5) yields for the bulk modulus K depending on the current void ratio e:

$$K = \frac{h_s}{3}\,\frac{\left[\ln\left(\frac{e_o}{e}\right)\right]^{(1/n)}}{\ln\left(\frac{1+e_o}{1+e}\right)}. \tag{A6}$$

In the initial stress free state, i.e. $p = 0$, $\varepsilon_{\mathrm{V}} = 0$ and $e = e_o$, the value of the bulk modulus is $K = 0$. With increasing compression the void ratio decreases, i.e. $e < e_o$, and the bulk modulus increases, $K > 0$, and for a vanishing void ratio, i.e. the volume cannot further compressed, the value of the bulk modulus tends asymptotically to $K \to \infty$ as $e \to 0$.

For the shear modulus, G, different functions are proposed in the literature. For instance, in the frequently applied empirical equation proposed by Hardin and

Drnevich [79] the shear modulus is a function of the current void ratio and the mean pressure, i.e.

$$G = G^* \frac{(2,97-e)^2}{(1+e)} \sqrt{\frac{p}{p_{atm}}}, \tag{A7}$$

where G^* is a material constant and p_{atm} denotes the atmospheric pressure.

Appendix B

The material parameter c can be calibrated either from the volume creep curve or from the stress relaxation curve. In the following the derivation of calibration procedures are demonstrated for four different cases. The quantities relevant for the calibration are illustrated in **Figure B1**. In **Case I** parameter c is related to the inclination of the volume creep curve at the beginning of creep, while in **Case II** the inclination of the volume creep curve at $\varepsilon_{V\infty}/2$ is considered. **Case III** and **Case IV** deals with the calibration of parameter c at two different states of the stress relaxation curves

B.1 Case I

Substituting the evolution Eq. (12) for the solid hardness into Eq.(5) one obtains for the rate of the volume strain under creep:

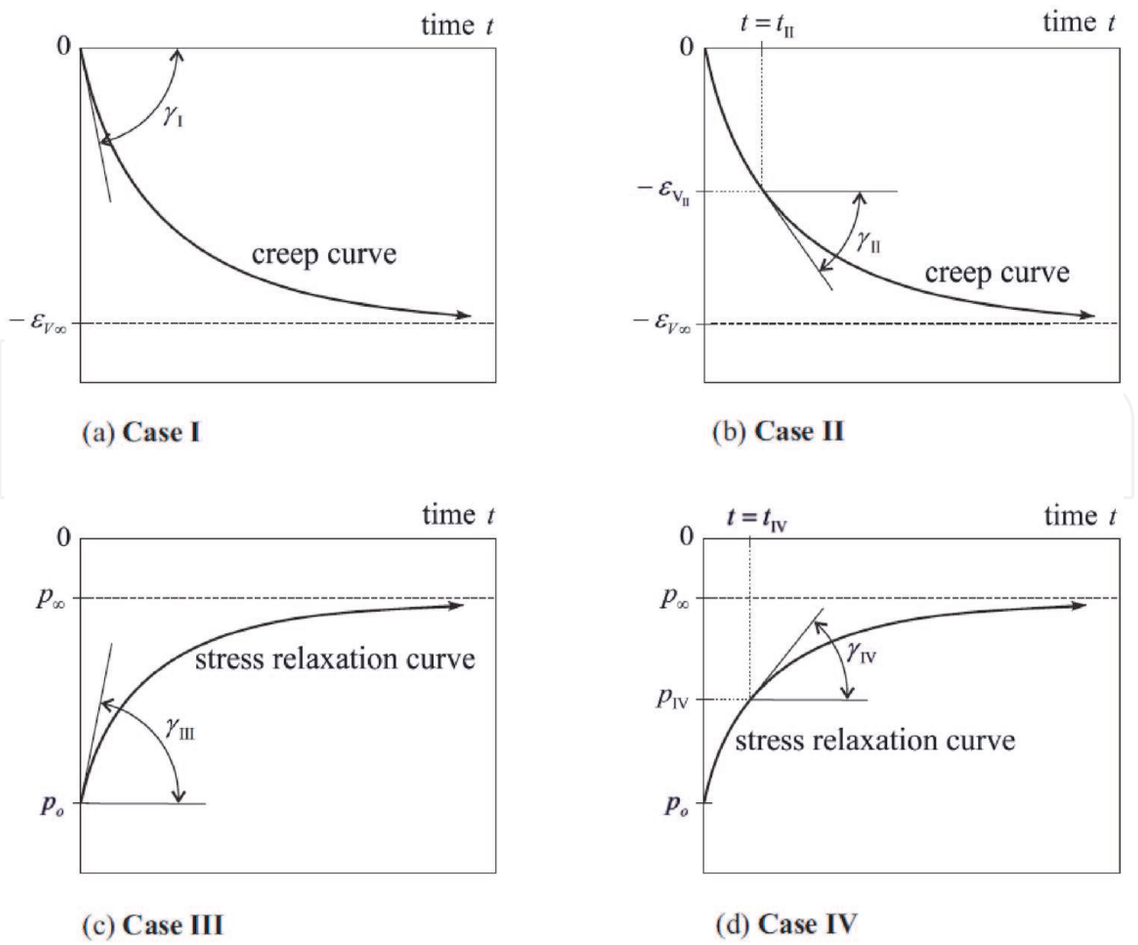

Figure B1.
Quantities at creep and stress relaxation curves relevant for the calibration.

$$\frac{\mathrm{d}\varepsilon_V}{\mathrm{d}t} = \dot{\varepsilon}_V = -\left(\frac{1}{c}\right)\frac{n\,e}{1+e}\left(\frac{3p_o}{h_{st}}\right)^n\left(1-\frac{h_{sw}}{h_{st}}\right). \tag{B1}$$

Herein the degraded solid hardness h_{sw} is defined for $h_{st}(t\to\infty) = h_{sw}$.

In **Case I** the inclination γ_{I} of the volume creep curve at the reference time $t = 0$ depends on the corresponding values of state quantities $e(t=0) = e_{\mathrm{I}}$; $p(t=0) = p_o$ and $h_{st}(t=0) = h_{st\,\mathrm{I}}$. From:

$$\tan\gamma_{\mathrm{I}} = -\left.\frac{\mathrm{d}\varepsilon_V}{\mathrm{d}t}\right|_{t=0} = \left(\frac{1}{c}\right)\frac{n\,e_{\mathrm{I}}}{(1+e_{\mathrm{I}})}\left(\frac{3p_o}{h_{st\,\mathrm{I}}}\right)^n\left(1-\frac{h_{sw}}{h_{st\,\mathrm{I}}}\right), \tag{B2}$$

one obtains for parameter c:

$$c = \frac{n\,e_{\mathrm{I}}}{\tan\gamma_{\mathrm{I}}(1+e_{\mathrm{I}})}\left(\frac{3p}{h_{st\,\mathrm{I}}}\right)^n\left(1-\frac{h_{sw}}{h_{st\,\mathrm{I}}}\right). \tag{B3}$$

B.2 Case II

In **Case II** the inclination γ_{II} of the volume creep curve is considered at time $t = t_{\mathrm{II}}$ where $\varepsilon_{\mathrm{V_{II}}} = \varepsilon_{V\infty}/2$; $e_{\mathrm{II}} = e(t=t_{\mathrm{II}})$ and $h_{st\,\mathrm{II}} = h_{st}(t=t_{\mathrm{II}})$. The asymptotic value $\varepsilon_{V\infty}$ can be estimated from the experiment. Then the corresponding relation for parameter c can be obtained from:

$$\tan\gamma_{\mathrm{II}} = -\left.\frac{\mathrm{d}\varepsilon_V}{\mathrm{d}t}\right|_{t=t_{\mathrm{II}}} = \left(\frac{1}{c}\right)\frac{n\,e_{\mathrm{II}}}{(1+e_{\mathrm{II}})}\left(\frac{3p_o}{h_{st\,\mathrm{II}}}\right)^n\left(1-\frac{h_{sw}}{h_{st\,\mathrm{II}}}\right) \tag{B4}$$

to:

$$c = \frac{n\,e_{\mathrm{II}}}{\tan\gamma_{\mathrm{II}}(1+e_{\mathrm{II}})}\left(\frac{3p}{h_{st\,\mathrm{II}}}\right)^n\left(1-\frac{h_{sw}}{h_{st\,\mathrm{II}}}\right). \tag{B5}$$

B.3 Case III

For stress relaxation under constant volume staring from $p(t=0) = p_o$ the rate of the mean stress according to Eq.(10) reads:

$$\dot{p} = p_o\left(\frac{\dot{h}_{st}}{h_{st}}\right). \tag{B6}$$

Substituting the evolution relation (12) for the solid hardness into Eq.(B6) one obtains:

$$\frac{\mathrm{d}p}{\mathrm{d}t} = \dot{p} = -\frac{p_o}{c}\left(1-\frac{h_{sw}}{h_{st}}\right). \tag{B7}$$

The inclination γ_{III} of the stress relaxation curve at the reference time $t = 0$ depends on the quantities $p(t=0) = p_o$ and $h_{st}(t=0) = h_{so}$. From:

$$\tan\gamma_{\mathrm{III}} = -\left.\frac{\mathrm{d}p}{\mathrm{d}t}\right|_{t=0} = \frac{p_o}{c}\left(1-\frac{h_{sw}}{h_{so}}\right) \tag{B8}$$

and with respect of Eq.(15), i.e. $h_{sw} = h_{so} p_\infty / p_o$, one obtains for parameter c:

$$c = \frac{p_o}{\tan \gamma_{\mathrm{III}}} \left(1 - \frac{p_\infty}{p_o}\right), \tag{B9}$$

where p_∞ denotes the asymptotic value of the stress relaxation curve for $t \to \infty$.

B.4 Case IV

As in experiments the inclination γ_{III} of the stress relaxation curve at the reference time $t = 0$ is difficult to measure an alternative calculation of parameter c is outlined in the following at $t = t_{\mathrm{IV}}$ and $p_{\mathrm{IV}} = (p_o + p_\infty)/2$. Then the corresponding rate of the solid hardness reads:

$$p_{\mathrm{IV}} = -\frac{p_{\mathrm{IV}}}{c} \left(1 - \frac{h_{sw}}{h_{st\,\mathrm{IV}}}\right), \tag{B10}$$

with:

$$h_{st\,\mathrm{IV}} = h_{st}|_{t=t_{\mathrm{IV}}} = \; h_{so} \frac{p_{\mathrm{IV}}}{p_o} \; = \frac{h_{so}}{2} \left(1 + \frac{p_\infty}{p_o}\right). \tag{B11}$$

Parameter c can be obtained from:

$$\tan \gamma_{\mathrm{IV}} = -\left.\frac{\mathrm{d}p}{\mathrm{d}t}\right|_{t=t_{\mathrm{IV}}} = \frac{p_{\mathrm{IV}}}{c} \left(1 - \frac{h_{sw}}{h_{so}} \frac{p_o}{p_{\mathrm{IV}}}\right) \tag{B12}$$

to:

$$c = \frac{(p_o + p_\infty)}{2 \tan \gamma_{\mathrm{IV}}} \left(1 - \frac{2 p_\infty}{(p_o + p_\infty)}\right). \tag{B13}$$

Appendix C

In order to embed the compression law (1) in a consistent manner into the hypoplastic constitutive Eq. (16) the rate of the mean pressure, i.e. $\dot{p} = -\dot{\sigma}_{ii}/3$, under monotonic isotropic compression starting from the maximum void ratio e_{i0} must coincide for both equations. For this particular compression path the void ratio $e(p) = e_i(p)$ and the scalar factors f_d, f_e, f_σ and $\hat{a}$ of the constitutive Eq. (16) result in the following values

$$\begin{gathered} f_d(e = e_i) = \left(\frac{e_{i0} - e_{d0}}{e_{c0} - e_{d0}}\right)^\alpha, \;\; f_e(e = e_i) = 1, \;\; f_\sigma(\sigma_{11} = \sigma_{22} = \sigma_{33}) = 3, \\ \text{and } \hat{a}(\sigma_{11} = \sigma_{22} = \sigma_{33}) = \frac{\sqrt{8/3} \;\; \sin \varphi_c}{3 - \; \sin \varphi_c}. \end{gathered} \tag{C1}$$

With respect to the relations in (C1) the rate of the mean pressure calculated from the hypoplastic constitutive Eq. (16) reads:

$$\dot{p}_{hypo} = -f_b \frac{\dot{e}_i}{3(1+e_i)} \left[\frac{8\ \sin^2\varphi}{(3-\ \sin\varphi)^2} + 1 - \frac{2\sqrt{2}\sin\varphi}{(3-\ \sin\varphi)} \left(\frac{e_{i0}-e_{d0}}{e_{c0}-e_{d0}} \right)^{\alpha} \right]. \quad \text{(C2)}$$

From the compression law (1) one obtains:

$$\dot{p}_{c\_law} = -\frac{\dot{e}_i}{e_i} \frac{h_s}{3n} \left(\frac{3p}{h_s} \right)^{(1-n)}. \quad \text{(C3)}$$

From the consistency condition $\dot{p}_{hypo} = \dot{p}_{c\_law}$, factor f_b can be determined, i.e.:

$$f_b = \frac{h_s\,(1+e_i)}{n\,e_i} \left[\frac{8\ \sin^2\varphi}{(3-\ \sin\varphi)^2} + 1 - \frac{2\sqrt{2}\sin\varphi}{(3-\ \sin\varphi)} \left(\frac{e_{i0}-e_{d0}}{e_{c0}-e_{d0}} \right)^{\alpha} \right]^{-1} \left(\frac{3p}{h_s} \right)^{(1-n)}. \quad \text{(C4)}$$

Appendix D – Symbols

D.1 State quantities

σ_{ij}	Effective Cauchy stress
e	Current void ratio
h_{st}	Solid hardness depending on the current state of weathering

D.2 Constitutive quantities

σ_{ij}^{∇}	Objective stress rate
$\dot{\varepsilon}_{ij}$	Strain rate
$\dot{\varepsilon}_V$	Volume strain rate, i.e. $\dot{\varepsilon}_V = \dot{\varepsilon}_{kk} = \dot{\varepsilon}_{11} + \dot{\varepsilon}_{22} + \dot{\varepsilon}_{33}$
$\dot{h}_{st}$	Degradation rate of the solid hardness
p	Mean effective pressure, i.e. $p = -\sigma_{kk}/3 = -(\sigma_{11} + \sigma_{22} + \sigma_{33})/3$
$\dot{p}$	Rate of the mean effective pressure
$\dot{e}$	Rate of the void ratio
e_i	Pressure dependent maximum void ratio
e_c	Pressure dependent critical void ratio
e_d	Pressure dependent minimum void ratio

D.3 Material parameters

h_s	Solid hardness of an unweathered material
h_{sw}	Asymptotical value of the degraded solid hardness for $t \to \infty$
c	Velocity dependent material parameter in the degradation law of the solid hardness
e_{i0}	Maximum void ratio at zero stress
e_{c0}	Critical void ratio at zero stress
e_{d0}	Minimum void ratio at zero stress
n	Material parameter in the compression law by Bauer
α	Material parameter of the hypoplastic constitutive equation
β	Material parameter of the hypoplastic constitutive equation

φ_c Critical friction angle
κ Material parameter of the enhanced hypoplastic constitutive equation

D.4 Initial values

e_o Initial void ratio
p_o Effective reference pressure
h_{so} Initial solid hardness at the reference time $t = 0$

Author details

Erich Bauer
Institute of Applied Mechanics, Graz University of Technology, Graz, Austria

*Address all correspondence to: erich.bauer@tugraz.at

References

[1] Justo J.L., Durand P. Settlement-time behaviour of granular embankments. International Journal for Numerical and Analytical Methods in Geomechanics. 2000, 24(3): 281–303.

[2] Hunter G., Fell R. Rockfill modulus and settlement of concrete face rockfill dams. Journal of Geotechnical and Geoenvironmental Engineering. 2003, 129(10): 909–917.

[3] Sowers G. F., Williams R. C., Wallace T. S. Compressibility of broken rock and settlement of rockfills. Proc. 6th ICSMFE, Montreal. 1965, Vol. 2: 561–565.

[4] Nobari E. S., Duncan J. M. Effect of reservoir filling on stresses and movements in earth and rockfill dams. Department of Civil Engineering, Report No. TE-72-1. University of California. 1972.

[5] Marsal R.J. Mechanical properties of rockfill. In: Embankment Dam Engineering. (eds.) Casagrande. R.C. Hirschfeld and S.J. Poulos, John Wiley & Sons, New York. 1973: 109–200.

[6] Alonso E., Oldecop L.A. Fundamentals of rockfill collapse. Proc. of the 1st Asian Conf. on Unsaturated Soils, eds. Rahardjo H., Toll DG., Leong EC., Balkema Press, Rotterdam. 2000, 3–13.

[7] Alonso E. E., Cardoso R. Behaviour of Materials for Earth and Rockfill Dams: Perspective from Unsaturated Soil Mechanics. Proceedings of the 2nd Int. Conf. on Long Term Behaviour of Dams, (eds.) Bauer, Semprich and Zenz, Publisher by Verlag der Technischen Universität Graz, ISBN 978–3–85125-070-1, 2009: 1–38.

[8] Wei Z., Xiaolin C., Chuangbing Z., Xinghong L. Creep analysis of high concrete-faced rockfill dam. International Journal for Numerical Methods in Biomedical Engineering. 2010, 26(11): 1477–1492.

[9] Brauns J., Kast K., Blinde A. 1980. Compaction Effects on the Mechanical and Saturation Behaviour of Disintegrated Rockfill. Proceedings of International Conference on Compaction, Paris. 1980, Vol. 1: 107–112.

[10] Oldecop L. A., Alonso E.E. 2007. Theoretical Investigation of the Time-Dependent Behaviour of Rockfill. Géotechnique. 2007, Vol. 57, N.3: 289–301.

[11] Oldecop L. A., de Agreda E. Testing Rockfill under Relative Humidity Control. Geotechnical Testing Journal. 2004, Vol. 27, N.3: 269–278.

[12] Zhang B. Y., Wang J. G., Shi R. F. Time-dependent deformation in high concrete-faced rockfill dam and separation between concrete face slab and cushion layer. Comput. Geotech. 2004, 31(7): 559–573.

[13] Modares M., Quiroz J.E. Structural analysis framework for concrete-faced rockfill dams. International Journal of Geomechanics. 2016, 16(1): 1–14.

[14] Cen W.J., Wen L.S., Zhang Z.Q., Xiong K. Numerical simulation of seismic damage and cracking of concrete slabs of high concrete face rockfill dams. Water Science and Engineering. 2016, 9(3): 205–211.

[15] Khosravi M., Li L., Bauer E. Numerical simulation of post-construction deformation of a concrete face rockfill dam. Proceedings of the 4th International Conference on Long-Term Behaviour and Environmentally Friendly Rehabilitation Technologies of Dams, LTBD 2017, (eds.) Noorzad, A.,

Bauer, E., Ghaemian, M., Ebrahimian, B., Published by Verlag der Technischen Universität Graz, ISBN 978–3-85125-564-5, 2017: 307–314.

[16] Saberi M, Annan CD, Konrad JM. Numerical analysis of concrete-faced rockfill dams considering effect of face slab – cushion layer interaction. Canadian Geotechnical Journal. 2018, 55 (10): 1489–1501.

[17] Marsal R.J. Large-scale testing of rockfill materials. Journal of the Soil Mechanics and Foundations Division, ASCE. 1967, 93(2): 27–43.

[18] Hu W., Frossart E., Hicher P. Y., Dano C. A new method to evaluate the mechanical behavior of granular material with large particles. Theory and validation. Proceedings of the 2nd Int. Conf. on Long Term Behaviour of Dams, (eds.) Bauer, Semprich and Zenz, Publisher by Verlag der Technischen Universität Graz, ISBN 978–3–85125-070-1, 2009: 437–478.

[19] Ovalle C., Frossard E., Dano C., Hu W., Maiolino S., Hicher P.Y. The effect of size on the strength of coarse rock aggregates and large rockfill samples through experimental data. Acta Mechanica. 2014, Vol. 225(8): 2199–2216.

[20] Ham T.G., Nakata Y., Orense R., ASCE, M., Hyodo M. Influence of Water on the Compressive Behavior of Decomposed Granite Soil. Journal of Geotechnical and Geoenvironmental Engineering. 2010, Vol. 136, (5): 697–705.

[21] Zhang B., Chen T., Peng C., Qian X., Jie Y. Experimental Study on Loading-Creep Coupling Effect in Rockfill Material. Int. J. Geomech. 2017, 17(9): 04017059. DOI: 10.1061/(ASCE) GM.1943-5622.0000938

[22] Zhou X., Chi S., Jia Y. Wetting deformation of core-wall rockfill dams. Int. J. Geomechanics. 2019, 19(8), 4019084. https://doi.org/10.1061/(ASCE)GM.1943-5622.0001444. https://doi.org/10.1061/(ASCE)GM.1943-5622.0001444

[23] Yin Y., Wu Y., Zhang B., Ding Y., Sun X. Two-stage wetting deformation behaviour of rock-fill material. Environmental Geotechnics. 2019, https://doi.org/10.1680/jenge.18.00130

[24] Viswanath P., Das A. Behavioural Study on Geomaterial Undergoing Chemo-Mechanical Degradation. In: Prashant A., Sachan A., Desai C. (eds). Advances in Computer Methods and Geomechanics. Lecture Notes in Civil Engineering. 2020, Vol 55. Springer, Singapore. 305–314. https://doi.org/10.1007/978-981-15-0886-8_25

[25] Terzaghi K. Discussion on salt springs and lower bear river dams, Trans. ASCE 125 (2). 1960: 139–148.

[26] Ovalle C., Dano C., Hicher P.Y., Cisternas M. Experimental framework for evaluating the mechanical behavior of dry and wet crushable granular materials based on the particle breakage ratio. Canadian Geotechnical Journal. 2015, Vol. 52: 587–598, https://doi.org/10.1139/cgj-2014-0079.

[27] Brauns J., Kast K., Blinde A. Compaction Effects on the Mechanical and Saturation Behavior of Disintegrated Rockfill. Proc. Int. Conf. on Compaction, Paris. 1980, Vol. 1: 107–112.

[28] Kast K. Mechanisches Verhalten von Granitschuettungen. Veröffentlichungen des Institutes für Bodenmechanik und Felsmechanik der Universität Fridericiana in Karlsruhe, Heft 125. 1992. (in German)

[29] Oldecop L.A., Alonso E.E. A model for rockfill compressibility. Géotechnique. 2001, Vol. 51, N.2: 127–139.

[30] Zhou W., Hua J., Chang X.L., Zhou C. Settlement analysis of the Shuibuya concrete-face rockfill dam. Computers and Geotechnics. 2011, 38: 269–280.

[31] Hu W., Yin Z., Dano C., Hicher P.Y. A constitutive model for granular materials considering grain breakage. Science China Technological Sciences. 2011, 54(8): 2188–2196.

[32] Fu Z.Z., Chen S.S., Liu S.H. Hypoplastic constitutive modelling of the wetting induced creep of rockfill materials. Sci China Tech Sci. 2012, 55: 2066–2082.

[33] Frossard E., Dano C., Hu W. Rockfill shear strength evaluation: A rational method based on size effects. Géotechnique. 2012, 62(5): 415–427.

[34] Xiao Y., Liu H., Chen Y. Testing and modeling of the state-dependent behaviors of rockfill material. Computers and Geotechnics. 2014, 61: 153–165.

[35] Xiao Y., Liu H., Chen Y., Jiang J. Bounding Surface Plasticity Model Incorporating the State Pressure Index for Rockfill Materials. J. Eng. Mech. 2014, 140(11): 04014087. DOI:10.1061/(ASCE)EM.1943-7889.0000802

[36] Alonso E. E. Fracture mechanics and rockfill dams". Soils and Rocks, An International Journal of Geotechnical and Geoenvironmental Engineering, São Paulo. 2014, 37(1): 3–35.

[37] Fu Z., Chen S., Peng C. Modeling cyclic behavior of rockfill materials in a framework of generalized plasticity. International Journal of Geomechanics. 2014, DOI:10.1061/(ASCE)GM.1943-5622.0000302, 191–204

[38] Wen L., Chai J., Xu Z., Qin Y., Li Y. Monitoring and numerical analysis of behaviour of Miaojiaba concrete-face rockfill dam built on river gravel foundation in China. Computers and Geotechnics. 2017, 85: 230–248.

[39] Tosun H., Tosun T.V. Dynamic Analysis of Embankment Dams under Strong Seismic Excitation and a Case Study. Proceedings of the 4th International Conference on Long-Term Behaviour and Environmentally Friendly Rehabilitation Technologies of Dams, LTBD 2017. Noorzad, A., Bauer, E., Ghaemian, M., Ebrahimian, B. (eds.), Published by Verlag der Technischen Universität Graz, ISBN 978–3–85125-564-5 2017: 747–753.

[40] Xu M., Jin D., Song E., Shen D. A rheological model to simulate the shear creep behavior of rockfills considering the influence of stress states Acta Geotechnica. 2018, 13:1313–1327. https://doi.org/10.1007/s11440-018-0716-8

[41] Wen L., Chai J., Xu Z., Qin Y.,Li Y. A statistical review of the behaviour of concrete-face rockfill dams based on case histories. Geotechnique. 2018, 68 (9): 749–771.

[42] Fu Z.Z., Chen S.S., Wie K.M. A generalized plasticity model for the stress-strain and creep behavior of rockfill materials. Science China Technological Sciences. 2019, 62, 649–664. Doi: 10.1007/s11431-018-9362-3

[43] Xu M., Jin D., Song E., Shen Z., Yang Z., Fu J. Full-scale creep test and back-analysis of the long-term settlement of heavy-loaded shallow foundations on a high rockfill embankment. Computers and Geotechnics. 2019, 115: 103156.

[44] Yao F.H., Guan S.H., Yang H., Chen Y., Qiu H.F., Ma G., Liu Q.W. Long-term deformation analysis of Shuibuya concrete face rockfill dam based on response surface method and improved genetic algorithm. Water Science and Engineering. 2019, 12(3): 196–204.

[45] Liu S., Sun Y., Shen C., Yin Z. Practical nonlinear constitutive model for rockfill materials with application to rockfill dam. Computers and Geotechnics. 2020, https://doi.org/10.1016/j.compgeo.2019.103383.

[46] Zhou X., Chi S., Wang M., Jia Y. Study on wetting deformation characteristics of coarse granular materials and its simulation in core-wall rockfill dams. Int J Numer Anal Methods Geomech. 2020, 44: 851–873. DOI: 10.1002/nag.3042

[47] Bauer E. Hypoplastic Modelling of Moisture-Sensitive Weathered Rockfill Materials. Acta Geotechnica. 2009, Vol. 4, (4): 261–272.

[48] Bauer E., Fu Z., Liu S. Constitutive Modelling of Rheological Properties of Materials for Rockfill Dams. In: Proceedings of the 6th International Conference on Dam Engineering, Lisbon, Portugal, February 15–17, 2011, eds. C. Pina, E. Portela, J. Gomes. Published by: CI-Premier Pte Ltd (Singapore), ISBN: 978–981–08-7896-2 (CD ROM): 1–14.

[49] Bauer E., Fu Z. Modeling of weathered and moisture sensitive granular materials. In: Advances in Bifurcation and Degradation in Geomaterials, Proceedings of the 9th International Workshop on Bifurcation and Degradation in Geomaterials, eds. S. Bonelli, C. Dascalu, F. Nicot. Springer Series in Geomechanics & Geoengineering, ISBN 978–94–007-1420-5, e-ISBN: 978–94–007-1421-2. 2011: 331–336.

[50] Bauer E., Fu Z., Liu S. Influence of pressure and density on the rheological properties of rockfills. Frontiers of Structural and Civil Engineering, 6, DOI 10.1007/s11709-012-0143-0. 2012: 25–34.

[51] Bauer E. Constitutive Modelling of Wetting Deformation of Rockfill Materials. International Journal of Civil Engineering. 2019, 17: 481–486. https://doi.org/10.1007/s40999-018-0327-7, Online ISSN 2383–3874, Print ISSN 1735–0522

[52] Bauer E., Safikhani S., Li L. Numerical simulation of the effect of grain fragmentation on the evolution of microstructure quantities. Meccanica. 2019, 54(4): 631–642. DOI 10.1007/s11012-019-00953-0 , ISSN 0025–6455

[53] Fu Z.Z., Bauer E. Hypoplastic Constitutive Modelling of the Long Term Behaviour and Wetting Deformation of Weathered Granular Materials. Proc. of the 2nd Int. Conference on Long Term Behaviour of Dams, Graz, Austria, eds. Bauer, E., Semprich, S. Zenz, G., ISBN: 978–3–85125-070-1. 2009: 473–478.

[54] Bauer E., Fu Z., Liu S. Hypoplastic Constitutive Modeling of Wetting Deformation of Weathered Rockfill Materials. Frontiers of Architecture and Civil Engineering in China. 2010, Vol. 4, (1): 78–91.

[55] Fu Z.Z., Chen S.S., Liu S.H. Hypoplastic constitutive modelling of the wetting induced creep of rockfill materials. Science China Technological Sciences. 2012, 55, (7): 2066–2082.

[56] Khosravi M., Li L., Safikhani S., Bauer E. Numerical simulations of the wetting effect on the long-term behavior of concrete face rockfill dams. Proceedings of the 5th International Symposium on Dam Safety, Istanbul, Turkey. 2018: 989–997.

[57] Bauer E. Constitutive Modelling of Critical States in Hypoplasticity. In: Proceedings of the Fifth International Symposium on Numerical Models in Geomechanics, Davos, Switzerland, Balkema. 1995: 15–20.

[58] Bauer E. Calibration of a comprehensive hypoplastic model for

granular materials. Soils and Foundations. 1996, 36(1): 13–26.

[59] Bauer E., Huang W., Wu W. Investigation of shear banding in an anisotropic hypoplastic material. Solids and Structures. 2004, 41: 5903–5919.

[60] Li L., Wang Z., Liu S., Bauer E. Calibration and performance of two different constitutive models for rockfill materials. Water Science and Engineering. 2016, 9(3): 227–239. http://dx.doi.org/10.1016/j.wse.2016.11.005

[61] Tejchman J., Bauer E. Numerical simulation of shear band formation with a polar hypoplastic constitutive model. Comput. Geotech. 1996, 19: 221–44.

[62] Huang W., Nübel K., Bauer E. A polar extension of hypoplastic model for granular material with shear localization. Mechanics of Materials. 2002, 34: 563–576.

[63] Huang W., Bauer E. Numerical investigations of shear localization in a micro-polar hypoplastic material. Int. J. for Numerical and Analytical Methods in Geomechanics. 2003, 27: 325–352.

[64] Ebrahimian B., Bauer E. Numerical simulation of the effect of interface friction of a bounding structure on shear deformation in a granular soil. Int. J. Numer. Anal. Meth. Geomech. 2012, 36 (12): 1486–1506.

[65] Bauer E., Li L., Huang W. Hypoplastic Constitutive modelling of grain damage under plane shearing. In Bifurcation and Degradation of Geomaterials in the New Millennium. 2015: 181–187.

[66] Bauer E., Li L., Khosravi M. Modelling grain damage under plane strain compression using a micro-polar continuum". In Proceedings of the 11th International Workshop on Bifurcation and Degradation in Geomaterials Dedicated to Hans Muhlhaus, Limassol, Cyprus, 21–25 May 2017, Papamichos, E., Papanastasiou, P., Pasternak, E., Dyskin, A. (eds.), Springer Series in Geomechanics and Geoengineering, DOI 10.1007/978-3-319-56397–8. 2017: 539–546.

[67] Bauer E. Modelling Grain Fragmentation in Hypoplasticity. Springer Nature Switzerland AG 2019, W. Wu (Ed.): Desiderata Geotechnica, SSGG. 2019: 1–20.

[68] Bauer E., Safikhani S. Numerical Investigation of Grain Fragmentation of a Granular Specimen under Plane Strain Compression. ASCE, Int. J. Geomech. 2020, 20(3): 04020007 DOI: 10.1061/(ASCE)GM.1943-5622.0001608.

[69] Gudehus G. A Comprehensive Constitutive Equation for Granular Materials. Soils and Foundations. 1996: 36, (1): 1–12.

[70] Yamamuro J.A., Bopp P.A., Lade P. V. One-dimensional compression of sands at high pressures. J. Geotech. Engrg., ASCE. 1996, 122 (2): 147–154.

[71] Laufer I. Grain crushing and high-pressure oedometer tests simulated with the discrete element method. Granul. Matter. 2015, 17(3): 389–412. http:// dx.doi.org/10.1007/s10035-015-0559-z.

[72] Fu R., Hua X., Zhou B. Discrete element modeling of crushable sands considering realistic particle shape effect. Computers and Geotechnics. 2017, 91, 179–191.

[73] Jaky J. Pressure in silos. Proc. 2nd International Conference on Soil Mechanics and Foundation Engineering, Rotterdam, Nederland. 1948, Vol. 1: 103–107.

[74] Matsuoka H., Nakai T. Stress-Strain Relationship of Soil Based on the SMP. Proceedings of 9th ICSMFE, Constitutive Equations of Soils. 1977: 153–162.

[75] Schofield A.N., Wroth C.P. Critical State Soil Mechanics, McGraw-Hill, London. 1968.

[76] Bauer E. Conditions for embedding Casagrande's critical states into hypoplasticity. Mechanics of Cohesive-Frictional Materials. 2000 Vol. 5: 125–148.

[77] Fu H., Ling H. Experimental research on the engineering properties of the fill materials used in the Cihaxia concrete faced rockfill dam. Research Report, Nanjing Hydraulic Research Institute, Nanjing, China. 2009 (in Chinese).

[78] Li G.X. Triaxial wetting experiments on rockfill materials used in Xiaolangdi earth dam. Research report from Tsinghua University. 1988.

[79] Hardin B. O., Drnevich V. P. Shear Modulus and Damping in Soils: Design Equations and Curves. J. Soil Mech. Found. Div. Proc. ASCE. 1972, Vol. 98, No. 7: 667–692.